CEAS-GNC-2022-018

CEAS EuroGNC 2022
"Conference on Guidance, Navigation and Control"
3-5 May 2022 @ Technische Universität Berlin, Germany

Output-Feedback Tube Model Predictive Control for Robust Autonomous Descent and Landing on Asteroids

Thomas Frekhaug Phd student, Universidad de Carlos III, Aerospace and Biology, 28911, Leganes, Spain. tfrekhau@ing.uc3m.es

Manuel Sanjurjo-Rivo Professor, Universidad de Carlos III, Aerospace and Biology, 28911, Leganes, Spain. msanjurj@ing.uc3m.es

Manuel Soler Professor, Universidad de Carlos III, Aerospace and Biology, 28911, Leganes, Spain. masolera@ing.uc3m.es

ABSTRACT

An output-feedback tube based model predictive controller is formulated and proposed for a real-time and fully autonomous descent and landing scenario onto small bodies and asteroids. With computational power being limited on deep space probes, the proposed guidance and control method relies solely on solving a quadratic optimisation problem online. Robustness is achieved through the off-line design of robust positively invariant sets, whereby the spacecraft is guaranteed to follow a nominal trajectory as generated from the solution of the quadratic optimisation problem. A full design synthesis of the tube based controller is proposed, accounting for both model and measurement uncertainties. Simulations verify the robustness of the strategy, but also highlights important challenges when limited to only linear systems in a highly nonlinear environment.

Keywords: MPC, Robust-Control, Autonomous

Notation

A polytopic set is denoted by bold math script, $\mathbb{X}$, represented through its half-plane representations $\mathbb{X} := \{x \in \mathbb{R}^n | Ax \leq b\}$. The addition of two polytopic sets are given as the minkowski sum, $\mathbb{X} \oplus \mathbb{Y} = \{x+y | x \in \mathbb{X}, y \in \mathbb{Y}\}$. The subtraction of two polytopic sets is similarly represented as the pontryagin difference $\mathbb{X} \ominus \mathbb{Y} = \{x | x \oplus \mathbb{Y} \subseteq \mathbb{X}\}$. Subscript k, as in x_k, represents discrete time, whereas the subscript i, as in x_i represents future predicted value. In the case where both is needed x_k^i, then i is given as superscript. Finally, accented variables, $\bar{(\cdot)}, \hat{(\cdot)}, \tilde{(\cdot)}$, represent vectors of similar dimensions as base.

1 Introduction

Landing onto small bodies and asteroids pose several challenges for Guidance, Navigation and Control (GNC). The environment is highly nonlinear due to irregularities in gravitational fields, together with other forces such as solar pressure and third body perturbations. Estimation of the true position and velocity of a spacecraft around small bodies and asteroids are also non-trivial, and as a result, a proposed GNC system should not only be robust to significant modelling errors, but also to estimator uncertainties. Additionally, small body operations usually occur in deep space with significant communication delays, and a GNC system that is independent and able to operate autonomously under such conditions is desirable.

Of recent missions, Hayabusa2 performed a touch-and-go on the near Earth asteroid Ryugu in 2019, where a partial ground, partial onboard strategy of the GNC for a powered descent onto the asteroid was utilised [1]. NASA's Osiris-Rex similarly successfully performed a touch-and-go on the asteroid Bennu in 2020, utilising a series of set-point onboard calculated braking manoeuvres in order to follow a pre-calculated trajectory onto the surface [2]. Whereas both missions were successful, the reliance on ground control and lack of autonomous adaptability indicates room for improvement. Future autonomous GNC methodologies for powered descent should have the onboard ability to adapt under uncertain and unexpected flight conditions, together with computational tractability and robust performance [3]. Recent reviews of GNC for small bodies highlight the necessity of a transition from offline to online computability, but also the need of improved robustness due to the higher degrees of uncertainties in small body environments [4, 5]. Similarly, whereas current practical applications of small body operations rely on separating the guidance and control algorithms, advances in optimisation-based algorithms makes them more attractive for the guidance and control within the aerospace field, especially for small body operations [6–8].

Model Predictive Control (MPC) is an optimisation based guidance and control algorithm that has been attracting increased research interest as a computational approach for descent and landing [9]. MPC solve the guidance and control problem in real-time through successive solution of optimization problems, subject to operational state and input constraints. For this, convex problems are advantageous due to numerous reasons, among others, faster solution times and the guaranteed existence of global solutions. Yet few problems are of an innate convex nature, and the problem of descent and landing is no exception. As such, the application of optimization based GNC methodologies have warranted several convexification techniques, enabling proposal of fully convex strategies. The authors of [10] proposed a convex Second Order Cone Program (SOCP) for a fuel-optimal trajectory for asteroid descent and landing. Similarly, [11] proposed a SOCP problem in combination with classical MPC. A quaternion six-degree-of-freedom MPC for precision landing has also been demonstrated in [12]. Convex MPC has further been shown to efficiently solve both circumnavigation and precision landing with superior constraint performance when compared to more traditional approaches [13]. Whereas [11] utilised a SOCP based MPC, a computationally simpler Quadratic Problem (QP) based MPC with robustness guaranteed through utilisation of robust tubes has been shown to solve the descent and landing problem in the presence of model uncertainties [14]. With increased availability of efficient solvers for convexified problems, among both SOCP and QP [15], the use of optimisation based guidance and control algorithms on spacecrafts are becoming more tractable.

For a guidance and control methodology to be applicable, it should not only be robust towards modelling uncertainties, but also to measurement and estimator uncertainties. With output feedback, the authors of [13] utilised an input observer to correct uncertainties while utilising MPC for the descent and landing. Negative interactions between the observer and MPC reduced the effectiveness of this approach. Crucially, for predictive methodologies, uncertainties in the initial states may produce huge uncertainties in predicted future states, giving way for methods such as stochastic MPC [16]. Stochastic MPC allow for future prediction of uncertainties, at the expense of an increased computational cost. A

different approach leveraging the advantages of invariant sets is the so-called tube MPC. The tube MPC has been explored in the context of rendezvous [17], and similarly, [14] explored tube linear MPC with state-feedback in the scenario of asteroid descent and landing. This paper is an extension of [14] to the output-feedback scenario, utilising the advantages of invariant sets to contain the spacecraft trajectory along a predicted trajectory while subject to both model and estimator uncertainties.

The paper is structured as follows; Section 2 frames the problem of the asteroid descent and landing in the content used for this work. Section 3 presents theory on the Output-Tube MPC (OTMPC) that is used as the guidance and control system for the spacecraft. Section 4 contains the primary contribution of this paper, the adoption of the OTMPC to the scenario of asteroid descent and landing. Simulations showing the viability of the methodology are presented in section 5, for a final conclusion in section 6.

2 Problem Statement; Small Body Descent & Landing

The spacecraft is assumed to be equipped with thrusters providing propulsion along the principle axes. The target asteroid is assumed to be rotating at a non-insignificant fixed angular rate about its axis of largest inertia. The relative position and velocity vector of the spacecraft, $[r, v]$, is expressed in a rotating asteroid centred fixed frame, whereas a linearised coordinate system, with vector $[r_{\mathrm{r}}, v_{\mathrm{r}}]$, is aligned with the fixed frame, but shifted to a linearisation point $r = r_{\mathrm{r}} + r_{\mathrm{r},0}$. The equations of motion for the spacecraft in the fixed frame are given as

$$\ddot{r} = -2\omega \times \dot{r} - \omega \times (\omega \times r) + \nabla U(r) + \frac{T}{m}, \tag{1}$$

were T is the spacecraft thrust vector, ω is asteroid rotation vector, m is the mass of the spacecraft, and $\nabla U(r)$ is the gravitational forces. Several methodologies for representing the non-linear gravitational potential around small bodies exists, but for this research, the gravitational potential has been represented by a sum of a series of optimised mascons $U = G\sum_{i=1}^{N_m} \frac{m_i}{\boldsymbol{r_i}}$ [18], giving the gravitational forces as the derivative of the potential. Defining the collected state vector as $\xi(t) = [r(t), v(t)]^\top$, and assuming that other forces such as third body perturbations and solar pressure are negligible, the equations of motion can be written as

$$\dot{\xi}(t) = \begin{bmatrix} 0 & 1 \\ -2S(\mathbb{Z}) & -S(\mathbb{Z})^2 \end{bmatrix} \xi(t) + \begin{bmatrix} 0 \\ \nabla U(\boldsymbol{r}(t)) \end{bmatrix} + \begin{bmatrix} 0 \\ \frac{T(t)}{m} \end{bmatrix}, \tag{2}$$

where $S(\cdot)$ indicates a skew symmetric matrix. Linearising (2) at an artificial equilibria $(\xi_{\mathrm{r},0}, T_{\mathrm{r},0})$, gives a linearised set of equations in the linearised coordinate frame,

$$\dot{\xi}_r(t) = \left(\begin{bmatrix} 0 & 1 \\ -2S(\mathbb{Z}) & -S(\mathbb{Z})^2 \end{bmatrix} + \nabla\nabla U(r(t))|_{r=r_{r,0}} \right) \xi_r(t) + \begin{bmatrix} 0 \\ \frac{T_r(t)}{m} \end{bmatrix} + w, \tag{3}$$

where w is a vector of model uncertainties stemming from the linearisation procedure. Furthermore, the linearised equations of motion is discretised with a timestep Δ_t using an exact discretization method. The discrete prediction error w_k represents the combined discrete model uncertainties of the linear system (3), compared to (2), and is contained in the set $\mathbb{W}$ (5).

The state estimator is assumed to be a non-specific estimator, be it an extended Kalman filter or other, of which return a reasonable state estimate $\hat{\xi}$ of the state ξ. Furthermore, the estimator is assumed to be in steady-state and assumed to be bounded within upper and lower bounds. As such, the state estimate may be defined as $\hat{\xi} = \xi + \nu$, $\nu \in \mathbb{V}$, where $\mathbb{V}$ is an outer-bounding hyperrectangle containing

the estimator uncertainty.

$$\hat{\xi} \in \xi \oplus \mathbb{V}, \quad \mathbb{V} := \{v | A_{\mathbb{V}} v \leq b_{\mathbb{V}}\} \tag{4}$$
$$w \in \mathbb{W}, \quad \mathbb{W} := \{w | A_{\mathbb{W}} w \leq b_{\mathbb{W}}\} \tag{5}$$

The matrices $A_{\mathbb{V}}$, $A_{\mathbb{W}}$, $b_{\mathbb{V}}$, and $b_{\mathbb{W}}$ are matrices appropriately chosen that reflect the bounds on the model and estimator uncertainties. The measurement noise is assumed to be randomly distributed within a subset of (4).

The initial state of the spacecraft is assumed to be either in a stable orbit, or in a trajectory that is not irrecoverable. Furthermore, the goal of the spacecraft is to safely hover as close as possible to a predefined landing point on the surface. Geometrically, the position is constrained to the convex intersection of a rectangular outer set and a pyramidic convex set with its apex at the desired landing spot, as shown in Fig. 1. Similarly, to fully constrain the state and thrust vectors, the velocity and thrust are bounded by rectangular sets, giving the constraint sets for the state and thrust as

$$\xi \in \mathbb{X}, \quad \mathbb{X} := \{\xi | A_{\mathbb{X}} \xi \leq b_{\mathbb{X}}\} \tag{6}$$
$$T \in \mathbb{U}, \quad \mathbb{U} := \{T | A_{\mathbb{U}} T \leq b_{\mathbb{U}}\}, \tag{7}$$

where $A_{\mathbb{X}}$, $A_{\mathbb{U}}$, $b_{\mathbb{X}}$, and $b_{\mathbb{U}}$ are appropriately chosen matrices.

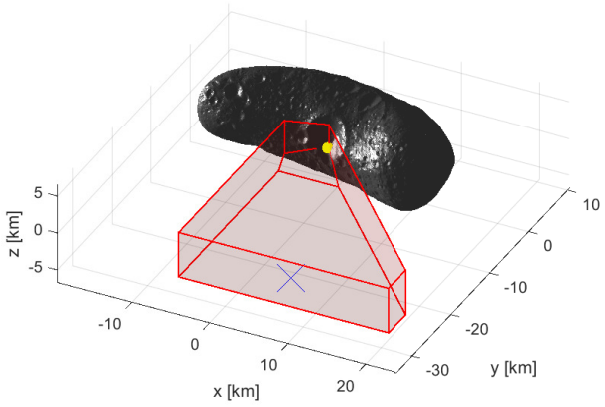

Fig. 1 State space for a powered descent on Eros. Surface target as yellow dot, starting point as blue cross.

3 Output-Tube Based MPC

Consider a nominal discrete disturbance free approximation of the state ξ, expressed in the linearised frame, denoted as $\bar{\xi} = [\bar{r}, \bar{v}]$, with corresponding set of equations given as the disturbance-free variant of (3). The error dynamics between the nominal and true dynamics, $e_k = \xi_{k,r} - \bar{\xi}$, are given by

$$\begin{aligned} e_{k+1} &= A\xi_{k,r} + BT_k + w_k - A\bar{\xi} - B\bar{T}_k \\ &= Ae_k + B(T_k - \bar{T}_k) + w_k. \end{aligned} \tag{8}$$

With the tube MPC feedback law from [19], the input applied to the true system dynamics becomes $T_k = \bar{T}_k + K_{\text{dr}} e_k$, which gives the closed loop error dynamics as

$$e_{k+1} = (A + BK_{\text{dr}})e_k + w_k, \tag{9}$$

of which, by the selection of K_{dr} such that $(A+BK_{\text{dr}})$ Hurwitz, converge to a Robust Positively Invariant (RPI) set of the system,

Definition 3.1 (RPI)**.** For an autonomous system, the set $\mathbb{Z}$ is considered an RPI set for the system $x_{k+1} = Ax_k + w_k$ and constraint set $\mathbb{X}$,$\mathbb{W}$, if $\mathbb{Z} \subseteq \mathbb{X}$ and $Ax_k + w_k \in \mathbb{Z} \forall x_k \in \mathbb{Z} \wedge \forall w_k \in \mathbb{W}$. $\mathbb{Z}$ is contained in all other RPI sets, then it is the minimal RPI. Similarly, if it contains all RPI sets, it is the Maximal RPI

I.e, once the trajectory enters the RPI set $\mathbb{Z}$, it will never leave the set. By choosing a feedback gain K_{dr} that minimises the volume of the minimum RPI, the system is guaranteed to exponentially approach a tube, defined by $\mathbb{Z}$, centred around a nominal trajectory generated by the nominal system. Therefore, consider the following quadratic optimisation program as a solution of the nominal system, subject to a quadratic cost,

$$(\bar{\xi}_{i=0}, \bar{T}_{i=0}) = \min_{\bar{\xi},\bar{T}} \quad \bar{\xi}_{i=N}^{\top} P_{\text{f}} \bar{\xi}_{i=N} + \sum_{i=0}^{N-1} \bar{\xi}_i^{\top} Q \bar{\xi}_i + \bar{T}_i^{\top} R \bar{T}_i \tag{10a}$$

s.t.

$$\bar{\xi}_{i+1} = A\bar{\xi}_i + B\bar{u}_i, \qquad \forall i \in \{0, N-1\}; \tag{10b}$$

$$\bar{T}_i \in \bar{\mathbb{U}} = \mathbb{U} - K_{\text{dr}}\mathbb{Z}, \qquad \forall i \in \{0, N-1\}; \tag{10c}$$

$$\bar{\xi}_i \in \bar{\mathbb{X}} = \mathbb{X} - \mathbb{Z}, \qquad \forall i \in \{0, N\}; \tag{10d}$$

$$\bar{\xi}_{i=0} = \xi_k \ominus \mathbb{Z}; \tag{10e}$$

$$\bar{\xi}_{i=N} \in \bar{\mathbb{X}}_f = \mathbb{X}_f - \mathbb{Z}, \tag{10f}$$

where $\bar{\xi}, \bar{T}$ is the nominal state and input, $\mathbb{Z}$ is an RPI set, preferably the minimal, for the error dynamics (9), P_{f} is the infinite horizon cost as given by the Ricatti equation, and $\mathbb{X}_f$ is a terminal set. The MPC for the nominal system is thus given by solving the optimisation problem at each discrete step $t = k$. After each successive solve, the input $T_k = \bar{T}_k^{i=0} + K_{\text{dr}}(\xi_{k,r} - \bar{\xi}_k^{i=0})$ is applied to the true system. With this, convergence of the true system to the terminal set is guaranteed with guaranteed constraint satisfaction [19].

The introduction of a state estimator adds to the uncertainty of the system that needs consideration. The authors of [20] extended the results of the state-feedback tube MPC design by coupling the estimator and state dynamics, showing convergence to an RPI for both error and estimator dynamics. However, the design procedure is not easily extended to larger systems due to increased dimensionality of the problem. Following the procedures of [21], consider instead an estimator in steady-state, giving an estimate of the state ξ as $\hat{\xi} = \xi \oplus \mathbb{V}$, where $\mathbb{V}$ is a convex, compact set that contains the origin, as defined in Eq. (4). Similarly, consider $\tilde{\xi}$ to be a candidate of the estimate $\hat{\xi}$, to be determined. Before proceeding, some notational summary, the pair (ξ_k, T_k) is the true state and input, $(\bar{\xi}_k, \bar{T}_k)$ is the nominal state and input, $\hat{\xi}_k$ is an estimate of the true state ξ_k, and $\tilde{\xi}_k$ is a candidate of the state estimate to be determined. As state feedback is no longer available, the output tube-based control law must be modified to reflect the use of a state estimate. This gives $T_k = \bar{T}_k^{i=0} + K_{\text{dr}}(\hat{\xi}_{k,r} - \bar{\xi}_k^{i=0})$, which, when applied to Eq. (8), gives the output-feedback error dynamics as

$$e_{k+1} = (A + BK_{\text{dr}})e_k + BK_{\text{dr}}\mathbb{V} + w_k, \tag{11}$$

$$= (A + BK_{\text{dr}})e_k + \Delta, \tag{12}$$

where $\Delta = BK_{\text{dr}}\mathbb{V} + w_k$ is the combined uncertainty of the error dynamics. Following similar arguments as with the state-feedback scenario, the true state ξ, with its estimate $\hat{\xi}$ may be shown to robustly follow the nominal trajectory given by ξ.

However, when progressing from k to $k+1$, it is not necessarily guaranteed that the estimate $\hat{\xi}_{k+1}$ is inside the predicted tube. That is, it is guaranteed that $\xi_{k+1} \in \hat{\xi}_{k+1} \oplus \mathbb{V}$, and that $\xi_{k+1} \in \bar{\xi}_k^{i=1} \oplus \mathbb{Z}$, but not that $\hat{\xi}_{k+1} \in \bar{\xi}_k^{i=1} \oplus \mathbb{Z}$. In such a scenario, the state estimate may appear to be outside the state boundaries, which in turn would make the nominal optimisation problem (10) infeasible. The authors of [21] proposes that there exists a candidate estimate $\tilde{\xi}_k$, such that a feasible solution is guaranteed at all time. Defining I_k to be the intersection of the predicted tube from the previous time step and the uncertainty of the estimate $\hat{\xi}_k$, that is $I_k = (\bar{\xi}_{k-1}^{i=1} \oplus \mathbb{Z}) \cap (\hat{\xi}_k \oplus \mathbb{V})$, then the candidate estimate $\tilde{\xi}_k$ may be chosen in accordance with the constraints

$$I_k \subseteq \tilde{\xi}_k \oplus \mathbb{V}, \tag{13}$$
$$I_k \subseteq \bar{\xi}_k^{i=0} \oplus \mathbb{Z}. \tag{14}$$

Including the candidate estimate as an optimization variable, subject to the constraints of I_k, the output-feedback nominal MPC may be formulated as

$$(\tilde{\xi}, \bar{\xi}_{i=0}, \bar{T}_{i=0}) = \min_{\tilde{\xi}, \bar{\xi}, \bar{T},} \quad \bar{\xi}_N^\top P_\mathrm{f} \bar{\xi}_N + \sum_{i=0}^{N-1} \bar{\xi}_i^\top Q \bar{\xi}_i + \bar{T}_i^\top R \bar{T}_i \tag{15a}$$

s.t.

$$\bar{\xi}_{i+1} = A\bar{\xi}_i + B\bar{T}_i, \qquad \forall i \in \{0, N-1\} \tag{15b}$$
$$\bar{T}_i \in \bar{\mathbb{U}} = \mathbb{U} - K_\mathrm{dr}\mathbb{Z}, \qquad \forall i \in \{0, N-1\} \tag{15c}$$
$$\bar{\xi}_i \in \bar{\mathbb{X}} = \mathbb{X} - \mathbb{Z}, \qquad \forall i \in \{0, N\} \tag{15d}$$
$$\bar{T}_{i=0} + K_\mathrm{dr}(\tilde{\xi} - \bar{\xi}_{i=0}) \in \mathbb{U}, \tag{15e}$$
$$\tilde{\xi} = \bar{\xi}_{i=0} \oplus \mathbb{Z}, \tag{15f}$$
$$\bar{\xi}_{i=N} \in \bar{\mathbb{X}}_f = \mathbb{X}_f - \mathbb{Z}, \tag{15g}$$
$$I_k \subseteq \tilde{\xi} \oplus \mathbb{V}, \tag{15h}$$
$$I_k \subseteq \bar{\xi}_{i=0} \oplus \mathbb{Z}, \tag{15i}$$

which is slightly more computationally expensive, compared to (10), due to the added constraints and candidate estimate. Also note that the replacement of $\hat{\xi}$ with $\tilde{\xi}$ allows for the explicit formulation of the output tube feedback law in (15e). For a further details on the output tube MPC, the reader is referred to [21].

4 Realisation of OTMPC for Descent and Landing

Due to limitations of available computational power on deep space probes and spacecraft, the resulting quadratic optimisation problem should be as simple as possible. Thus, the following will discuss the adoption and design of the aforementioned output-feedback based tube MPC to the descent and landing scenario.

4.1 Disturbance rejection and RPI

Using the linear dynamics of Eq. (3), it is necessary to determine the smallest possible RPI, ideally the minimal one. An arbitrary ε close approximation is possibly using the methods of [22], however, the number of vertices and facets explodes rapidly with minkowski-sums, making this approach not feasible in higher dimensions. Additionally, significant complexity to the optimisation program is added with the large half-plane representations of exact RPI's. Other methods exists, but at the cost of either complexity in the number of constraints, or in the challenge of choosing a suitable initial geometry [23]. For this

research, an RPI chosen as a geometric hyper rectangle is advantageous, as in a d-dimensional problem it may be represented by a limited set of $2d$-inequalities, keeping the complexity of the MPC at minimum. The hyper rectangle is fitted to a minimal ellipsoidal RPI which is computed by solving the following Linear Matrix Inequalities (LMI).

Considering the state feedback error dynamics Eq. (9), an RPI must satisfy both $\mathbb{Z} = \{x | x_k^\top P x_k \leq 1\}$ and $\mathbb{Z} = \{x | x_{k+1}^\top P x_{k+1} \leq 1\}$. Requiring that $\bar{\mathbb{X}} = \mathbb{X} - \mathbb{Z}$ and $\bar{\mathbb{U}} = \mathbb{U} - K_{\text{dr}}\mathbb{Z}$ is not empty sets, and minimising the volume of of the ellipsoidal RPI, [19] showed that an ellipsoidal RPI may be found by solving an LMI. However, with output-feedback, the disturbance is dependent on the choice of K_{dr}, extending the LMI to a bilinear matrix inequality. A simple two step extension of [19] is proposed to find a suitable pair P and K_{dr}. First, solving the following LMI

$$\min_{Y, W_1, \gamma_1} \quad \gamma_1 \tag{16a}$$

$$\begin{bmatrix} \lambda_1 W_1 & * & * \\ 0 & 1-\lambda_1, * & \\ AW_1 + BY & w_{V_i} & W \end{bmatrix} > 0, \quad \forall \mathbb{W}_{V_i} \in \Delta \tag{16b}$$

$$\begin{bmatrix} \rho^2 & l_j^\top Y \\ * & W_1 \end{bmatrix} > 0, \quad i = 1, ..., n_{ru} \tag{16c}$$

$$\begin{bmatrix} 1 & h_j^\top W_1 \\ * & W_1 \end{bmatrix} > 0, \quad j = 1, ..., n_{rx} \tag{16d}$$

giving $K_{\text{dr}} = YW_1$, then the RPI, given by a symmetric shape matrix P, under the disturbance $\Delta = w + BK_{\text{dr}}\mathbb{V}$ may be found by solving the following similar LMI

$$\min_{W_2, \gamma_2} \quad \gamma_2 \tag{17a}$$

$$\begin{bmatrix} \lambda_2 W_2 & * & * \\ 0 & 1-\lambda_2, * & \\ AW_2 + BKW_2 & \Delta_{V_i} & W_2 \end{bmatrix} > 0, \quad \forall \Delta_{V_i} \in \Delta \tag{17b}$$

$$\begin{bmatrix} 1 & h_j^\top W_2 \\ * & W_2 \end{bmatrix} > 0, \quad j = 1, ..., n_{rx} \tag{17c}$$

Thus, the set $\mathbb{Z}$, defined by a hyperrectangle constructed from the eigenvectors of $P_2 = W_2^{-1}$ is an RPI for the autonomous system Eq. (12). In the LMI's (16) and (17), the parameters $(\lambda_1, \lambda_2) \in (0, 1)$ ensure convexity, stemming from the s-procedure, whereas the parameter $\rho \in (0, 1)$ ensures that the set $\mathbb{U} - BK_{\text{dr}}\mathbb{Z}$ is non-empty. Finally, l, h are vectors from the state and input constraint, written as $\mathbb{X} = \{\xi \quad | \quad |h_i^\top \xi|_1 \leq 1, i \in 1, ..., n_\xi\}$, $\mathbb{U} = \{T \quad | \quad |l_i^\top T|_1 \leq 1, i \in 1, ..., n_u\}$,.

4.2 Model and measurement uncertainty

The model uncertainty $\mathbb{W}$ must be an outer approximation of the true uncertainty, and is not often easily determined. A direct direct approach is possible, where $\mathbb{W}$ is calculated directly from (3) and (2) along with maximum bounds on state and input values. Similarly, for the first order Taylor approximation used in this paper, the uncertainty may be determined by evaluating the second order Taylor at maximum bounds of the states state-space. However, neither will yield an exact knowledge about the model uncertainty as the true gravitational potential is rarely precisely known, together with additional other forces. For this paper, the model uncertainty has been determined as the worst case prediction error given by the linearised model in the high fidelity environment. Using worst case scenarios, the pre-

viously mentioned methods may also return a suitable envelope for the model uncertainty in a realistic scenario. It should be noted that, whereas this work only considers gravitational forces as non-linearities, other possible additional non-linear forces in a higher fidelity environment should also be captured by the design of $\mathbb{W}$.

Additionally, bounds on the uncertainty of the estimator is also required. Following [13], the estimate is initially considered to randomly distributed around the true state by a box limited by $[b_{\mathbb{V},r}, b_{\mathbb{V},v}]^\top \approx [1/3, 0.5/3]^\top \gamma$, where $\gamma \leq 1$ is a scaling parameter to increase or decrease the uncertainty of the estimate. From [24], it is clear that this order of uncertainty or better is feasible using an extended Kalman filter with landmark based measurements.

4.3 Selection of $\mathbb{Z}$

In the output-feedback scenario, the error dynamics uncertainty is no longer easily defined, as it depends on the choice of feedback gain K_{dr}. Prioritizing a small RPI to suppress model uncertainty may increase the controller induced uncertainty $BK_{\text{dr}}\mathbb{V}$ of the error feedback system, leaving $K_{\text{dr}}\mathbb{Z} \ominus \mathbb{U}$ small with possible minimal improvements of the RPI. Similarly, prioritizing manoeuvrability such that $K_{\text{dr}}\mathbb{Z} \ominus \mathbb{U}$ is large, the suppression of model uncertainty through control becomes challenging. As an example, for the scenario later proposed in the simulations, one possible RPI where $\bar{\mathbb{U}}$ is non-empty and large for the given linearised dynamics is shown geometrically in Fig. 2. The model uncertainty in this scenario becomes dominating, whereas the nominal manoeuvrability, as seen by the set $\mathbb{U}$, is large, it is clear that resulting RPI is also large. This presents the most significant challenge of the output tube MPC.

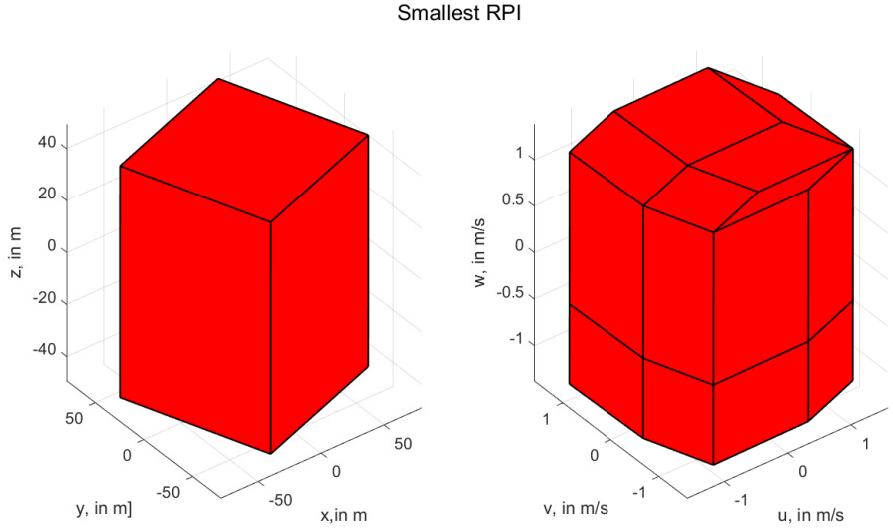

Fig. 2 The smallest RPI found, projected in *r* on the left, and *v* on the right.

4.4 OTMPC for descent and landing

For the practical implementation of the quadratic optimisation problem in the 3-degree-of-freedom descent and landing scenario, some modifications to the OTMPC are warranted. The terminal constraint Eq. (15g) is commonly omitted during practical applications of MPC, as it is challenging to determine the feasible region of the MPC. As such, a cost on the state transition, and a sufficiently large terminal cost is necessitated in order to implicitly satisfy the terminal constraint. Furthermore, due to the state space $\mathbb{X}$ being much larger than the reachable set of the MPC, the prediction horizon N is chosen sufficiently large, such that the spacecraft is able to stop within the prediction horizon. This is important in scenarios where a state constraint is inactive at one discrete time, but active in the next. The cost function is further

modified to $(\bar{\xi}_{i=N}-\xi_{l,r})^\top P(\bar{\xi}_{i=N}-\xi_{l,r})+\sum_{i=0}^{N-1}(\bar{\xi}_i-\xi_{l,r})^\top Q(\bar{\xi}_i-\xi_{l,r})+\bar{T}_i^\top R\bar{T}_i$ such that the optimum cost is shifted to the desired landing site, in order to drive the nominal system to the landing site $\xi_{l,r}$. With this, the quadratic optimisation program may be given as

$$(\tilde{\xi},\bar{\xi}_{i=0},\bar{T}_{i=0}) = \min_{\tilde{\xi},\bar{T}} \quad (\bar{\xi}_{i=N}-\xi_{l,r})^\top P_{\mathrm{f}}(\bar{\xi}_{i=N}-\xi_{l,r})+\sum_{i=0}^{N-1}(\bar{\xi}_i-\xi_{l,r})^\top Q(\bar{\xi}_i-\xi_{l,r})+\bar{T}_i^\top R\bar{T}_i \tag{18a}$$

s.t.

$$\bar{\xi}_{i+1} = A\bar{\xi}_i + B\bar{T}_i, \qquad \forall i\in\{0,N-1\}, \tag{18b}$$
$$\bar{T}_i \in \bar{\mathbb{U}} = \mathbb{U}-K_{\mathrm{dr}}\mathbb{Z}, \qquad \forall i\in\{0,N-1\}, \tag{18c}$$
$$\bar{\xi}_i \in \bar{\mathbb{X}} = \mathbb{X}-\mathbb{Z}, \qquad \forall i\in\{0,N\}, \tag{18d}$$
$$\bar{T}_{i=0}+K_{\mathrm{dr}}(\tilde{\xi}-\bar{\xi}_{i=0})\in\mathbb{U}, \tag{18e}$$
$$\tilde{\xi} = \bar{\xi}_{i=0}\oplus\mathbb{Z}, \tag{18f}$$
$$I_k \subseteq \tilde{\xi}\oplus\mathbb{V}, \tag{18g}$$
$$I_k \subseteq \bar{\xi}_{i=0}\oplus\mathbb{Z}, \tag{18h}$$

where $I_k = (\bar{\xi}_{k-1}^{i=1}\oplus\mathbb{Z})\cap(\hat{\xi}_k\oplus\mathbb{V})$.

5 Simulation

Consider the scenario of the descent and landing on the asteroid Eros, visited in a fly-by mission by Near Shoemaker in 2000. Assuming the spacecraft mass is 2000kg, the maximum thrust along each principle axis being 50N, a prediction horizon $N=60$, and discrete time $\Delta_t = 20$s. Two scenarios have been considered, with the first scenario starting in a 32km, 0° inclination orbit, similar to [14]. The second scenario is a Monte-Carlo simulation where the initial orbits are randomized. Both scenarios targets a safe landing at the same point on the asteroid surface.

The initial scenario considers two different RPI designs. Initially, the the RPI was selected as a in Fig. 2, such as to allow for manoeuvrability of the spacecraft, at cost of increased tube volume. The second RPI was chosen as the opposite, prioritizing a smaller RPI volume, at the expense of a smaller nominal input volume $\mathbb{U}$. In Fig. 3, the error dynamics (12) in the first scenario is presented for the larger RPI. The advantage of the constraint (18f) is seen, as the initial nominal state $\bar{\xi}_k^{i=0}$ has been selected such as to maximise the available geometry of the RPI. In turn, this allows the controller to utilise more of the available input, i.e not only being limited to the set $\bar{\mathbb{U}}$. This effect becomes more evident when compared to the input trajectory presented in Fig. 5, where the nominal input set $\mathbb{U}$ is smaller than the nominal input set seen in Fig. 4. Whereas the difference in the nominal volume is large, both trajectories have almost full utilisation of the true input set.

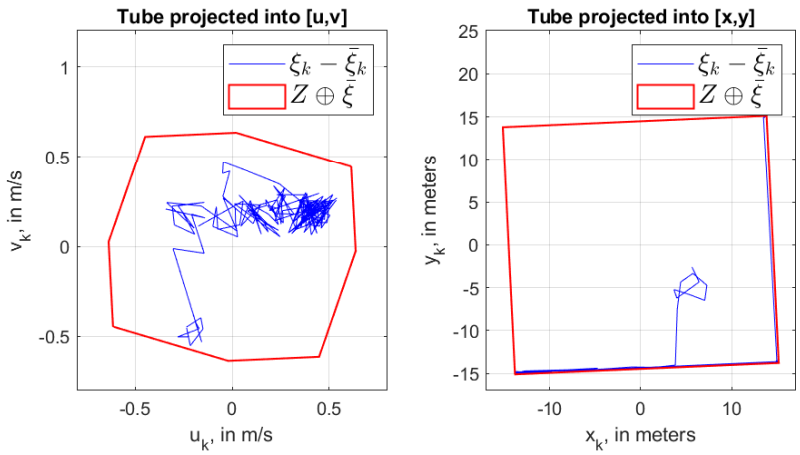

Fig. 3 The projection of the RPI in x, y and corresponding velocities u, v

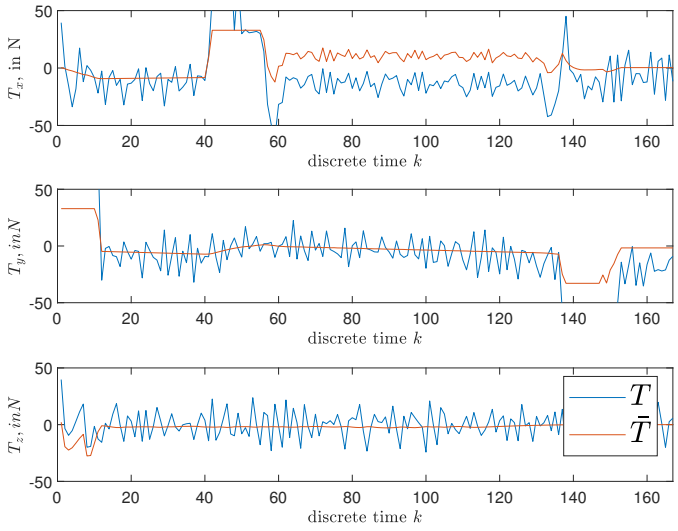

Fig. 4 Spacecraft thrust vector over time. $\bar{T}$ is the thrust generated by the optimisation problem (18), T is the realization of the thrust

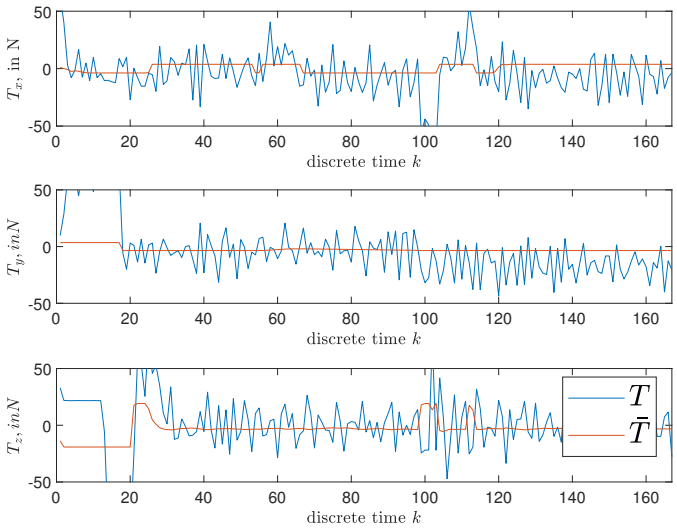

Fig. 5 $\bar{T}$ **is the thrust generated by the optimisation problem** (18)**,** T **is the thrust applied to the system. In this scenario, the thrust is much more susceptible to disturbances**

A brief discussion of the choice of disturbance sets $\mathbb{W}$ and $\mathbb{V}$ is also warranted. By poor selection of either, the total combined model and induced estimator uncertainty $\Delta = \mathbb{W} \oplus BK_{\text{dr}}\mathbb{V}$ may exceed the a-priori selected bounds, and there is no longer guarantees that the state ξ will remain in the tube. For these results, the estimator uncertainties was by definitions always confined to be within $\mathbb{V}$. The uncertainty model was selected from a Monte-Carlo analysis of the performance of the linear models. Fig. 6 shows the combined model uncertainty and controller induced uncertainty, in a selection of dimensions, and it is clear that for these results, the uncertainty sets have been appropriately selected, i.e not overly conservative nor infeasible. The performance of the controller may only be guaranteed as long as the bounds are appropriately chosen. However, as the proposed selection of the RPI induces a degree of conservativeness, it is likely that small errors of the uncertainty sets will not induce a direct failure.

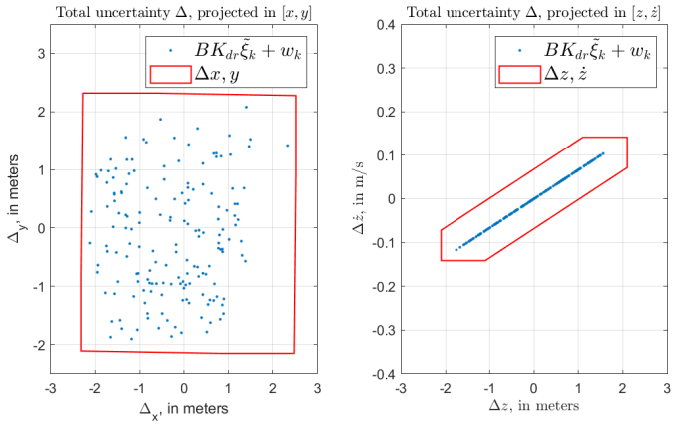

Fig. 6 The combined uncertainty from modelling errors and the additional prediction gained error from the estimate

The effect of the measurement uncertainty and selections of K_{dr} is clearly reflected in the input trajectory. With a smaller RPI, the the controller induced uncertainty, $BK_{\text{dr}}\mathbb{V}$, becomes larger. Similarly, a larger measurement uncertainty set $\mathbb{V}$ also induces higher controller uncertainties. This effect is evident in comparison of the the thrust trajectories of Fig. 4 and Fig. 5, where the latter has a smaller RPI for higher precision, at the expense of higher induced disturbances in the thrust trajectory.

The second scenario considers Monte-Carlo simulations where the initial orbits were randomized within the domain $\mathbb{X}$. In Fig. 7, it is clear that the spacecraft is able to successfully land on the surface given any feasible initial conditions. Due to the lack of bias compensation, the spacecraft will reach a terminal position set, centred around an equilibria as determined by (12). By enforcing a terminal condition, and having a shrinking horizon in the MPC, the steady-state error may be reduced to the RPI. Similarly, other approaches for bias compensation in MPC may readily be applied in this scenario, in order to drive the state towards an RPI centred around the target area.

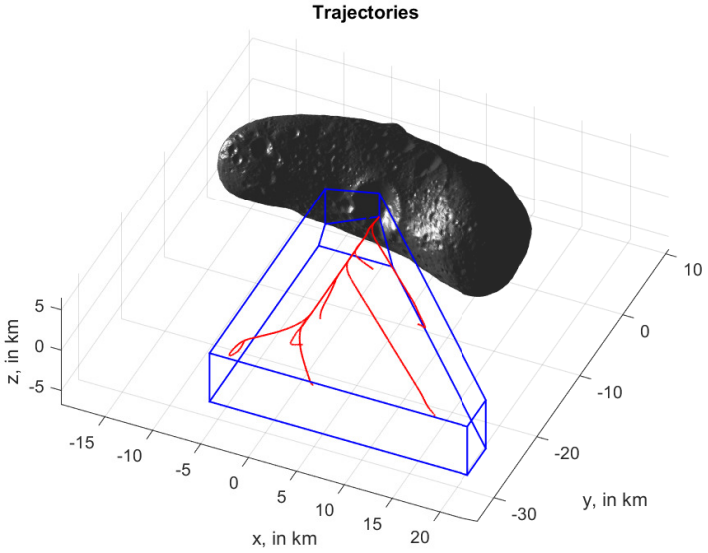

Fig. 7 Multiple trajectories from random initial conditions shows the lander, under the proposed guidance and control policy, safely reaching the surface.

6 Conclusion

With computational guidance and control, more powerful methodologies become viable, even in areas where computational power is limited. This paper has explored a robust rendition of utilising MPC in a quadratic form for its application to asteroid landing. It has been shown that a robust and computationally fast method, utilising only linear models and constraints in its online implementation, is able to robustly solve the asteroid descent and landing problem. The limitation of linear constraints and models does however induce a high degree of conservatism. It is clear that the tube based approach is performing adequately while having a guaranteed performance, but challenges still remain. The selection of the RPI set has the biggest impact on the performance of the linear tube based method. An iterative approach of solving the two-step LMIs presented was partially been explored for some results. Further research is warranted in the design and computation of feasible RPI-sets that is able to simultaneously account for both the measurement and model uncertainty. Currently, it is challenging to determine usable RPI's, even with minimal estimator uncertainty, without adding significant conservativeness.

References

[1] Go Ono, Fuyuto Terui, Naoko Ogawa, Yuya Mimasu, Kent Yoshikawa, Yuto Takei, Takanao Saiki, and Yuichi Tsuda. Design and flight results of gnc systems in hayabusa2 descent operations. *Astrodynamics*, 4(2):105–117, Jun 2020. DOI: 10.1007/s42064-020-0072-y.

[2] K. Berry, B. Sutter, A. May, K. Williams, Brent Barbee, M. Beckman, and Bobby Williams. Osiris-rex touch-and-go (tag) mission design and analysis. *Advances in the Astronautical Sciences*, 149:667–678, 01 2013.

[3] John M. Carson III, Michelle M. Munk, Behçet Açıkmeşe, and Ping Lu. Introduction to the virtual collection on autonomous guidance, navigation, and control for planetary entry, descent, and landing. *Journal of Guidance, Control, and Dynamics*, 44(3):456–456, 2021. DOI: 10.2514/1.G005947.

[4] Pedro Simplício, Andrés Marcos, Eric Joffre, Mattia Zamaro, and Nuno Silva. Review of guidance techniques for landing on small bodies. *Progress in Aerospace Sciences*, 103:69–83, 2018. DOI: https://doi.org/10.1016/j.paerosci.2018.10.005.

[5] Dantong Ge, Pingyuan Cui, and Shengying Zhu. Recent development of autonomous gnc technologies for small celestial body descent and landing. *Progress in Aerospace Sciences*, 110:100551, 2019. DOI: https://doi.org/10.1016/j.paerosci.2019.06.002.

[6] Danylo Malyuta, Yue Yu, Purnanand Elango, and Behçet Açıkmeşe. Advances in trajectory optimization for space vehicle control. *Annual Reviews in Control*, 52:282–315, 2021. DOI: https://doi.org/10.1016/j.arcontrol.2021.04.013.

[7] Runqi Chai, Antonios Tsourdos, Al Savvaris, Senchun Chai, Yuanqing Xia, and C.L. Philip Chen. Review of advanced guidance and control algorithms for space/aerospace vehicles. *Progress in Aerospace Sciences*, 122:100696, 2021. DOI: https://doi.org/10.1016/j.paerosci.2021.100696.

[8] Ping Lu. Introducing computational guidance and control. *Journal of Guidance, Control, and Dynamics*, 40(2):193–193, 2017. DOI: 10.2514/1.G002745.

[9] Utku Eren, Anna Prach, Başaran Bahadır Koçer, Saša V. Raković, Erdal Kayacan, and Behçet Açıkmeşe. Model predictive control in aerospace systems: Current state and opportunities. *Journal of Guidance, Control, and Dynamics*, 40(7):1541–1566, 2017. DOI: 10.2514/1.G002507.

[10] Robin Marie Pinson. *Autonomous optimal trajectory design employing convex optimization for powered descent on an asteroid*. PhD thesis, Iowa State University, January 2016.

[11] Julio C. Sanchez, Francisco Gavilan, and Rafael Vazquez. A predictive guidance algorithm for autonomous asteroid soft landing. *IFAC-PapersOnLine*, 51(12):6–11, 2018. IFAC Workshop on Networked and Autonomous Air and Space Systems NAASS 2018. DOI: https://doi.org/10.1016/j.ifacol.2018.07.080.

[12] Unsik Lee and Mehran Mesbahi. Constrained autonomous precision landing via dual quaternions and model predictive control. *Journal of Guidance, Control, and Dynamics*, 40(2):292–308, 2017. DOI: 10.2514/1.G001879.

[13] Dominic Liao-McPherson, William D. Dunham, and Ilya Kolmanovsky. *Model Predictive Control Strategies for Constrained Soft Landing on an Asteroid*. 2016. DOI: 10.2514/6.2016-5507.

[14] Thomas Frekhaug, Manuel Sanjurjo Rivo, and Manuel Soler. Tube-based robust model predictive control for asteroid soft landing. 06 2021. Global Space Exploration Conference.

[15] Jacob Mattingley and Stephen Boyd. Cvxgen: A code generator for embedded convex optimization. *Optimization and Engineering*, 13, 03 2012. DOI: 10.1007/s11081-011-9176-9.

[16] Francisco Gavilan, Rafael Vazquez, and Eduardo F. Camacho. Chance-constrained model predictive control for spacecraft rendezvous with disturbance estimation. *Control Engineering Practice*, 20(2):111–122, 2012. DOI: https://doi.org/10.1016/j.conengprac.2011.09.006.

[17] M. Mammarella, E. Capello, H. Park, G. Guglieri, and M. Romano. Tube-based robust model predictive control for spacecraft proximity operations in the presence of persistent disturbance. *Aerospace Science and Technology*, 77:585–594, 2018. DOI: https://doi.org/10.1016/j.ast.2018.04.009.

[18] Juan Garcia Bonilla, Pablo Machuca, and Manuel Sanjurjo-Rivo. Preprint: Small-body gravitational modeling for on-board operations and mass distribution estimation: Trade-off analysis and novel approach. 2021. 72nd International Astronautical Congress.

[19] D. Limon, I. Alvarado, T. Alamo, and E.F. Camacho. On the design of robust tube-based mpc for tracking. *IFAC Proceedings Volumes*, 41(2):15333–15338, 2008. 17th IFAC World Congress. DOI: https://doi.org/10.3182/20080706-5-KR-1001.02593.

[20] I. Alvarado, D. Limon, T. Alamo, and E.F. Camacho. Output feedback robust tube based mpc for tracking of piece-wise constant references. In *2007 46th IEEE Conference on Decision and Control*, pages 2175–2180, 2007. DOI: 10.1109/CDC.2007.4434772.

[21] Sankaranarayanan Subramanian, Sergio Lucia, and Sebastian Engell. A novel tube-based output feedback mpc for constrained linear systems. In *2017 American Control Conference (ACC)*, pages 3060–3065, 2017. DOI: 10.23919/ACC.2017.7963417.

[22] S.V. Rakovic, E.C. Kerrigan, K.I. Kouramas, and D.Q. Mayne. Invariant approximations of the minimal robust positively invariant set. *IEEE Transactions on Automatic Control*, 50(3):406–410, 2005. DOI: 10.1109/TAC.2005.843854.

[23] Paul Trodden. A one-step approach to computing a polytopic robust positively invariant set. *IEEE Transactions on Automatic Control*, 61(12):4100–4105, 2016. DOI: 10.1109/TAC.2016.2541300.

[24] Li Shuang and Cui Pingyuan. Landmark tracking based autonomous navigation schemes for landing spacecraft on asteroids. *Acta Astronautica*, 62:391–403, 03 2008. DOI: 10.1016/j.actaastro.2007.11.009.